ELSEVIER

Chemical Physics 244 (1999) 449–460

Chemical Physics

www.elsevier.nl/locate/chemphys

A method to obtain meV-collision-energy resolution in scattering studies: application to the $H + D_2 \rightarrow HD(\nu' = 0, j') + D(\theta_{rel} < 80^\circ)$ reaction at $E_{rel} = 1.275 \pm 0.011$ eV

Sharon Kennedy, Kushlani Dharmesena, Steven Moser, Marcis Auzinsh [1], Neil E. Shafer-Ray *

Department of Physics and Astronomy, The University of Oklahoma, Norman, OK 73019, USA

Received 19 November 1998

Abstract

Previous work has shown that a one-to-one correspondence between the speed and scattering angle of state-selected AB products of the gas-phase reaction sequence $AX + h\nu \rightarrow A + X$, $A + BC \rightarrow AB + C$ can be exploited to measure state-to-state differential cross-sections without resorting to molecular beams. Here we demonstrate a modification to this photoinitiated technique that enables for the observation of the forward- and backward-scattered products of a reaction with improved collision energy resolution. This modification is demonstrated by its application to the measurement of the j' dependence of the yield of forward-scattered HD product in the reaction $H + D_2 \rightarrow HD(\nu' = 0, j') + D$ at 1.275 ± 0.011 eV. The data obtained are consistent with quantum scattering calculations that do not include the geometric phase.

1. Introduction

A striking feature of recent studies of atom–diatom reactive scattering processes is the marked dependence of the reaction dynamics on the collision energy. As the collision energy is changed by a fraction of an electron volt, the mechanism of reaction may change from direct to complex-forming [1], from adiabatic to diabatic [2], or from insertion to abstraction [3]. These studies suggest that a high-resolution measurement of the energy dependence of a bimolecular collision could reveal a rich spectrum that would shed light on the varied mechanisms that contribute to reactivity.

Until now, state-to-state differential cross-sections of bimolecular reactions have been measured at only a few discrete collision energies and, with one exception [4–6], at a collision energy resolution of no better than $\pm 5\%$ of the collision energy. Here we present data taken with an apparatus that has the ability to measure state-to-state and scattering-angle-dependent cross-sections of reactive scattering processes with a resolution of $\pm 0.8\%$ of the collision energy. This precision is roughly equal to that

* Corresponding author.

[1] Present address. Department of Physics, University of Latvia, 19 Rainis blvd, Riga, LV - 1586, Latvia.

0301-0104/99/$ - see front matter
PII: S0301-0104(99)00139-1

of the best ($\pm 0.6\%$) ever reported in a measurement of the state-to-state cross-section of a bimolecular reactive scattering process [7]. The technique presented here is unique in its potential for combining the features of high collision energy resolution, its applicability to a wide variety of reactions, and its ability to study the state- and scattering-angle-dependent dynamics of a reaction as a continuous function of energy.

In this paper we apply our new technique to the study of $H + D_2$ reactive scattering at 1.275 ± 0.011 eV. Six years ago, disagreements between state-to-state integral cross-sections of the $D + H_2 \rightarrow HD(\nu', j') + D$ reaction measured by Adelman et al. [8] and predictions of theory [9] were resolved by the inclusion of the effect of a geometric phase shift resulting from the Jahn–Teller interaction between the ground and first excited state of the $D + H_2$ system [10]. However, in a recent study of the state-to-state differential cross-section of the $H + D_2$ reaction, Wrede and Schnieder [5] found no evidence for a dynamical resonance predicted by the calculations of Kuppermann and co-workers that incorporate the effect of the geometric phase [1]. Their measurements of the state-to-state differential cross-section of the *backward-scattered* HD product of the reaction, however, are consistent with several calculations that do not include the effect of the geometric phase shift [11–13]. Thus experimental data to date indicate that, although the geometric phase does influence the reaction dynamics, the nature of this influence is not yet completely understood. The results presented here for the *forward-scattered* HD product, although of limited scope, are consistent with the findings of Wrede and Schnieder.

The next section discusses our experimental strategy. Section 3 presents experimental details. Section 4 gives a numerical model of the experiment necessary to interpret the data obtained. Section 5 uses this analysis to compare the quantum theory of D'Mello and co-workers [14] to experiment. Section 6 summarizes our results.

2. Experimental strategy

Two methods have been applied successfully to the study of state-to-state differential cross-sections of bimolecular reactions. One method involves molecular beam machines. In these experiments a beam of one reactant is crossed with a beam containing the other reactant. The laboratory-frame velocity of the observed product is then used to infer the scattering angle (and, in some cases, the product state) of the reaction [15].

A second technique to observe product-state- and scattering-angle-dependent reaction probabilities probes the A + BC atom–diatom reaction by observing the diatomic product of the photoinitiated reaction sequence [2,16–29]

$$AX + h\nu \rightarrow A + X, \tag{1}$$

$$A + BC \rightarrow AB(\nu', j') + C. \tag{2}$$

The reaction is carried out in a single gas mixture containing AX and BC. The energetics of the AX photodissociation determine both the magnitude of the relative collision energy E_{rel} and the speed u of the center of mass of the A + BC system. After the reaction, the AB product is detected as a function of rotational–vibrational state by selective resonance-enhanced laser excitation [30]. Provided the reactant atoms A and product atoms C are produced in their ground states and the reactant BC molecule is cold, the speed u of the center of mass and the center-of-mass-frame speed u_{AB} of the $AB(\nu', j')$ product are determined by conservation of energy and momentum (see Appendix A). The laboratory-frame speed v_{AB} of the product, however, depends on the scattering angle, as shown in the Newton diagram of Fig. 1. For example, consider the $H + D_2 \rightarrow HD(\nu = 0, j' = 6) + H$ reaction at 1.275 eV. For this case, the backward-scattered HD product has a laboratory frame speed of 1.76 km s^{-1}, whereas the forward-scattered HD product has a laboratory-frame speed of 8.77 km s^{-1}. By measuring the speed of a state-selected HD product, sensitivity to the scattering angle can be obtained.

One advantage of the photoinitiated technique over the crossed-beam technique is a great increase in sensitivity. This increase in sensitivity has enabled the experimental determination of state-selective differential cross-section of the $H + D_2$ [27], $H + O_2$ [2,16,24], $O(^1D) + H_2$ [28], $Cl + CH_4$ [22,29], and $O(^1D) + N_2O$ [18,19] reactions. A second advantage is the ability to vary continuously the collision en-

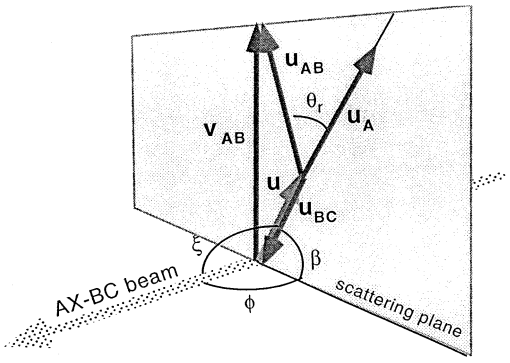

Fig. 1. Newton diagram for the state-to-state reaction A + BC → AB + C for $\boldsymbol{v}_{BC} = \boldsymbol{u}_{BC} + \boldsymbol{u} = \boldsymbol{0}$ is shown in the shaded plane. The Newton diagram illustrates the one-to-one correspondence between the laboratory frame speed v_{AB} and the scattering angle θ_r. Note that for $\theta_r = 0$ and $\theta_r = 180°$, $\boldsymbol{v}_{AB}$ is parallel to the direction of the relative velocity $\boldsymbol{u}_A - \boldsymbol{u}_{BC}$ of the reaction. Thus for backward- and forward-scattered reactions, the direction of the relative velocity may be constrained by constraining $\boldsymbol{v}_{AB}$. The orientation of the scattering plane with respect to the molecular beam defines an angle ϕ. If the products travel radially outward from a collimated molecular beam, the angle ξ between $\boldsymbol{v}_A$ and direction of the beam is determined by $\cos\xi = \cos\phi\cos\beta$, where β is a function of the scattering angle.

ergy by tuning the wavelength of the laser radiation used to photolyze the AX precursor. These experiments have, however, been carried out with relatively poor collision energy resolution. In what follows, we show that a hybrid of the molecular beam and photoinitiated techniques can reduce the collision energy resolution to the meV range.

In the technique presented here, a gas mixture of AX and BC is used to create a molecular beam inside a machine that allows laser radiation to be sent down an axis that is approximately parallel with the molecular beam. Laser radiation sent down this path photolyzes the AX precursor to initiate the A + BC reaction (Fig. 2a). After the A + BC reaction has occurred, the AB product is selectively detected as a function of its rotational and vibrational quantum state by resonance-enhanced multiphoton ionization (Fig. 2b). A pulsed field is then used to force the AB^+ ions to hit a microchannel plate detector (Fig. 2c). From the position that the ions hit the detector, the initial speed of the AB(v', j') product, and hence the scattering angle of the reaction is determined.

In an ideal world, the probe laser radiation could Doppler select only those products that are moving at the beam velocity. This would allow us to observe *only those products that travel radially outward from the beam*. Such selection would establish a one-to-one correspondence between ion speed and the center-of-mass-frame scattering angle and, as will be discussed, would improve the collision energy resolution. Unfortunately, our broad-band dye laser has very poor velocity selection. For the data presented here on $H + D_2$ reactive scattering, sensitivity to the position at which ions hit the detector is achieved by placing a metal strip (mask) in front of the detector. In this way we assure that only the fastest moving (forward-scattered) HD products are detected and that we observe products traveling radially outward from the molecular beam. (By 'radially outward' we mean in the radial direction with respect to a frame of reference that moves at the beam velocity.) In addition to limiting the observed scattering angles, the mask eliminates background caused by the slow-moving ions produced from nonresonant ionization processes.

This experimental strategy leads to improved collision energy resolution when compared to previous

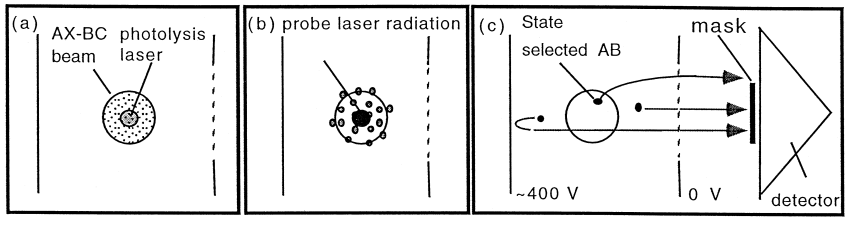

Fig. 2. Schematic of the perpendicular beam technique: (a) laser radiation copropagating with a cold molecular beam mixture of AX and BC is used to photolyze the AX precursor, initiating the A + BC reaction; (b) probe laser radiation is used to state selectively ionize AB(v', j') product; and (c) a pulsed voltage source is used to accelerate AB^+ ions toward a microchannel plate detector. Ions traveling with a sufficient vertical velocity to pass a rectangular mask are detected.

studies for two reasons. First, this experiment (like others [22,27]) occurs in a cold expansion of AX and BC. Second, our measurement is biased to favor reactions that occur with the relative velocity of the reactants directed radially outward from the molecular beam. Just as a Doppler-free spectroscopic measurement reduces the spread in velocities in the direction of a laser, collisions that occur in the radial direction have a reduced spread in the relative velocity between the A and BC reactants, and hence improved collision energy resolution.

3. Experimental

A simplified machine drawing of the vacuum apparatus used to carry out the $H + D_2$ study reported here is shown in Fig. 3. The system consists of a 6″ diffusion-pumped source chamber used to create the molecular beam, a 6″ diffusion-pumped ionization chamber in which the photoinitiated reaction takes place, and a 4″ diffusion-pumped detection chamber housing a microchannel plate detector. (Although the apparatus accommodates differential pumping between the source and ionization chambers, for the studies produced here the two chambers were not isolated.)

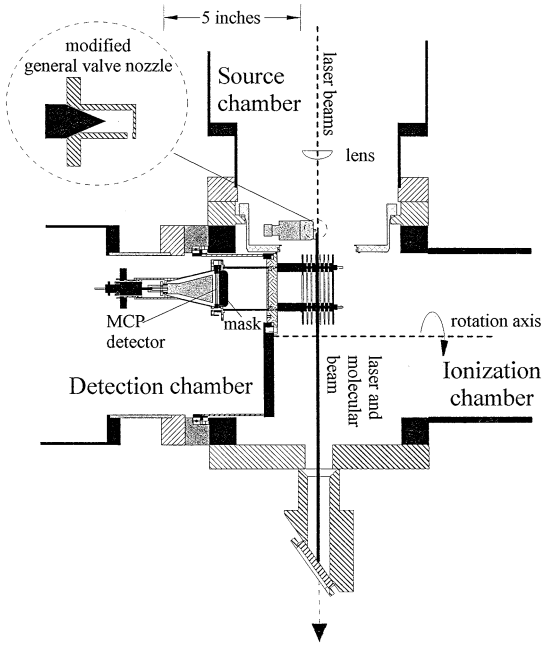

Fig. 3. Experimental apparatus.

Gas enters the source chamber through a General Valve nozzle (PV-9-563). This nozzle has been modified to allow gas to exit through a 0.3 mm outlet at right angles from the axis of the nozzle (Fig. 3, inset). The nozzle is backed by a room-temperature 1500 Torr mixture of HI (5%) and D_2(95%). The *ortho*- and *para*-D_2 rotational populations are fit well by a 233 K Boltzmann distribution. The valve operates at a 10 Hz repetition rate and the source and ionization chambers maintain an average pressure of 2×10^{-5} Torr whereas the detection chamber is at 2×10^{-6} Torr.

The nozzle design allows laser radiation to pass along an axis that is displaced 1 mm from the valve outlet. Dissociating laser radiation at 266 nm (the fourth harmonic of one of our two Nd:YAG laser lasers) is fired along this axis to initiate the reaction sequence

$$\mathrm{HI}(\nu = 0, j = 0\text{–}6) + h\nu(266\,\mathrm{nm}) \rightarrow \mathrm{H} + \mathrm{I}\left(^2\mathrm{P}_{3/2}\right), \quad (3)$$

$$\mathrm{H} + \mathrm{D}_2(\nu = 0, j = 0\text{–}4) \rightarrow \mathrm{HD}(\nu', j') + \mathrm{D}(E_{\mathrm{rel}} = 1.275\,\mathrm{eV}), \quad (4)$$

$$\mathrm{HD}(\nu' = 0, j') + 2h\nu(\sim 210\,\mathrm{nm}) \rightarrow \mathrm{HD}\left(\mathrm{E}, \mathrm{F}\,\Sigma_g^+\right) + h\nu \rightarrow \mathrm{HD}^+. \quad (5)$$

The intensity of the 266 nm pump laser radiation varies from 12 to 30 mJ. Probe laser radiation (400 μJ @ ~210 nm) is generated from the third harmonic of a Nd:YAG pumped dye laser system. This light is used to state-selectively ionize HD($\nu' = 0, j'$) molecules by E, F state-resonance-enhanced multiphoton ionization [31], where $j' = 6, 7, 8$, and 10. (The state $j' = 9$ was not studied because of interfering signal caused by $2 + 1$ ionization of atomic hydrogen. For $j' < 6$ a thermal background of HD made signal collection difficult, whereas for $j' > 10$, the yield of forward-scattered product was too small to observe.) The ions created by the probe laser are accelerated into a 74.6 mm long time-of-flight tube by a uniform 150 V cm^{-1} electric field. This uniform field is created after the lasers fire by applying a 395 V pulse to a 26.3 mm long stack of resistively

divided plates. After the ions travel down the time-of-flight tube, they encounter a microchannel-plate detector. A 12.5 mm mask is placed in front of this detector to limit our observation to quickly moving (forward-scattered) HD^+ molecules. This mask also completely blocks the contribution of signal from the slow hydrogen atoms from dissociation of HI that leads to excited-state $I(^2P_{1/2})$ atoms. By observing an increase in signal as the time delay between the dissociating 'pump' laser and the probe laser is increased, we confirm that the signal is from the reaction. The laser system operates at a repetition rate of 10 Hz. For observation of $HD(\nu' = 0, j' = 6)$ product, on average 20 product HD^+ ions are observed and one background ion is detected per laser shot.

4. Monte Carlo simulation

Experimental determination of the collision energy resolution of our experiment would require observation of a narrow resonance in a scattering processes. Short of obtaining such data, narrow collision energy resolution can be demonstrated either by the simple approximate model presented in Appendix B or by the detailed Monte Carlo simulation presented in this section. Because of the importance of our Monte Carlo simulation to the interpretation of our experimental data, great care has been taken to make it as realistic as possible. The simulation is a three-dimensional model that accounts for every aspect of the experiment, including the size and temporal width of the pump and probe laser radiation, delay between the pump and probe lasers, the spread in beam velocities, the disappearance of the photoproduct as a function of time, the rotational temperatures of the diatomic reactant and the photolytic precursor, the anisotropy of the dissociation, and the finite size of the microchannel plate detector. To create such a realistic model, over fifty experimental parameters must be specified. Fortunately, the vast majority of these parameters are known to well within the limits of the sensitivity of our measurement. The length of the time-of-flight tube, wavelength and bandwidth of the dissociation laser, rotational distribution of the D_2 reactant, temporal and spatial widths of the pump and probe lasers, and branching ratio for $I(^2P_{3/2})$ and $I(^2P_{1/2})$ formation in the dissociation of HI are just a few of these parameters. For the $H + D_2$ experiment presented in Section 5, only two parameters have yet to be measured with sufficient accuracy to completely determine the resolution of our apparatus. These are the spread in our beam velocity and the rotational distribution of the HI precursor.

For the simulations presented here, we estimate the spread in beam velocities and the rotational distribution of the HI precursor based on previous molecular beam work: We assume that our 2 atm pulsed expansion of a 5% HI/95% D_2 gas mixture through a 0.30 mm orifice leads to a beam velocity of $(2C_p k_B T/\overline{m})^{1/2} = 1100$ m s^{-1}, where C_p is the specific heat of an atomic gas, $T = 293$ K is the temperature of the HI/D_2 gas mixture before expansion, and $\overline{m}$ is the average mass of the particles in the beam. The applicability of this approximation to the expansion of H_2 gas has been demonstrated in Ref. [32]. The spread in beam velocity is taken to be 30% of the velocity of the beam, or ± 330 m s^{-1}. This is a conservative estimate based on the findings of Keil and co-workers [33]. The HI rotational distribution is assumed to be characterized by a temperature of 20 K. This temperature is similar to that of HCl observed in a similar pulsed expansion created by Simpson et al. [22].

4.1. Collision energy spread

The Monte Carlo determination of the distribution of collision energies in our measurement is shown by the heavy solid line in Fig. 4. It is centered around 1.275 eV and is approximately Gaussian with a full width at half maximum (FWHM) of 0.011 eV. Our measurement is not sensitive to a second distribution of collision energies centered at 0.53 eV corresponding to the production of $I(^2P_{1/2})$, because HD products of these low-energy collisions do not move quickly enough to pass the mask. In Table 1, the influence of various experimental parameters on the collision energy distribution is presented. The fact that no single variation has a dramatic effect on the resolution indicates that the value of 11 meV has many contributing factors. These factors include the

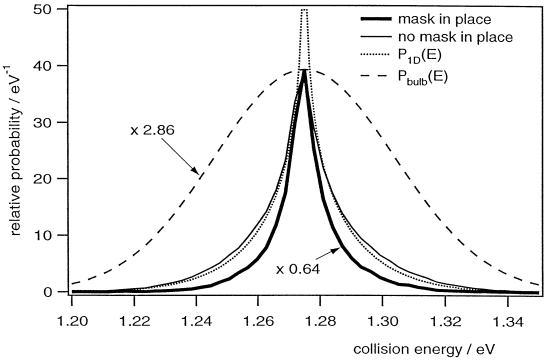

Fig. 4. Solid line: Collision energy resolution in our study of the $HI + h\nu \rightarrow H + I$, $H + D_2 \rightarrow HD + D$ reaction. Solid light line: Collision energy resolution expected if the mask of Fig. 2c were not in place. Dotted line: Collision energy resolution expected without the mask in place, as determined from the approximate form of $P_{1D}(E)$ given by Eq. (B.8) of the text. Dashed line: Collision energy resolution expected from a 'bulb' experiment using a HI/D_2 gas mixture with an 18.6 K Maxwell–Boltzmann velocity distribution.

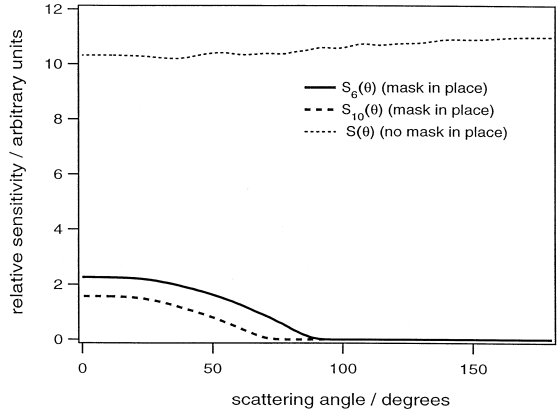

Fig. 5. Sensitivity to scattering angle in a our study of the $HI + h\nu \rightarrow H + I$, $H + D_2 \rightarrow HD(\nu' = 0, j') + D$ reaction for $j' = 6$ (solid lines) and $j' = 10$ (dashed lines.) The solid lines indicate the scattering-angle dependence of the experiment as carried out. The dotted line indicates the sensitivity in an experiment were the mask of Fig. 2 not in place.

detection of reactions at a distribution of scattering angles greater than 0°, imperfect collimation of the molecular beam, finite bandwidth of the Doppler probe laser, a slight misalignment of the laser beams with respect to the molecular beam, and the rotational temperature of the HI precursor.

When no mask is in place, we find no sensitivity to the direction of $\boldsymbol{v}_{AB}$. For this case, the distribution of collision energies may be approximated by the function $P_{1D}(E)$ derived in Appendix B (see Eq. (B.8)). This analytical approximation (Fig. 4, dotted line) agrees closely with the result of the Monte Carlo simulation (Fig. 4, light solid line) provided E is not too close to E_{rel}.

4.2. Scattering-angle-dependent sensitivity

As expected, the mask placed in front of the microchannel plate (see Figs. 2 and 3) greatly affects the sensitivity $S_{j'}(\theta)$ of the apparatus to scattering angle (Fig. 5). When the mask is in place, the measurement is most sensitive to the fastest-moving forward-scattered HD products. Comparison of the relative sensitivity to scattering angle for $HD(\nu' = 0, j' = 6)$ to that of $HD(\acute{\nu} = 0, j' = 10)$ shows an important j' dependence. Because $j' = 10$ products move more slowly than $j' = 6$ products, they are less likely to be detected when the mask is in place. If no mask is used, the measurement is nearly insensitive to both scattering angle and final rotational state.

Table 1
Effect of various parameters on the collision energy resolution in the photoinitiated reaction sequence $HI + h\nu \rightarrow H + I$, $H + D_2 \rightarrow HD(\acute{\nu} = 0, \acute{j} = 6)$ ($E_{rel} = 1.275$ eV)

Variable	Description	Hypothetical change in value	Resulting change in resolution	Resulting change in sensitivity
Δv_b	FWHM spread in the beam velocity	0.33 km s^{-1} → 0.11 km s^{-1}	11.0 meV → 6.7 meV	none
d_{source}	distance from the nozzle orifice to center of the detection region	45 mm → 135 mm	11.0 meV → 9.0 meV	reduced by 100
w	mask width	12.5 mm → 15 mm	11.0 meV → 9.0 meV	reduced by 4.4
T_{HI}	rotational temperature of the HI	20 K → 1 K	11.0 meV → 10.0 meV	none

5. Results

We now compare our experimental results to those expected from the state-to-state differential cross-sections of the $H + D_2$ reaction at 1.30 eV, as calculated by D'Mello and co-workers [14] and shown in Fig. 6. The j'-dependent signals we obtain are in clear disagreement with the cross-sections obtained from integrating these differential cross-sections over all angles, as can be seen in Fig. 7. This disagreement is expected, for we have measured the *forward-scattered* product of a process with a highly structured differential cross-section. To compare quantum theory to our data, we must convolute the theoretical cross-sections with the sensitivity function of our instrument:

$$D_{j'} = \int \frac{\mathrm{d}\sigma_{j'}}{\mathrm{d}\Omega} S_{j'}(\theta) \sin\theta \, \mathrm{d}\theta \,. \qquad (6)$$

Fig. 7 compares our data to the values of $D_{j'}$ obtained from convoluting D'Mello's differential cross-sections with our j'-dependent instrument function (i.e., from integrating the product of the dashed lines and solid lines of Fig. 6 over $\sin\theta \, \mathrm{d}\theta$, as indicated by Eq. (6)). Both the experimental data and the theoretical predictions have been normalized to one. No experimental parameters were adjusted to make this comparison. The error bars on the experimental data correspond to one standard deviation of the mean obtained from nine measurements of the distribution, but do not include the contribution of possible systematic errors. Agreement of this forward convolution of theory with our experimental

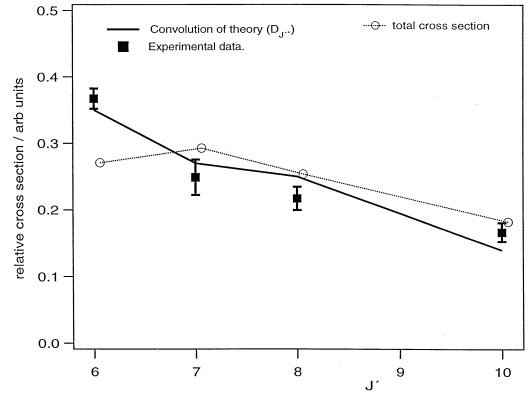

Fig. 7. Squares: Experimental cross-section for the $H + D_2 \rightarrow HD(\nu' = 0, j') + D$ reaction at 1.275 ± 0.011 eV. Heavy solid line: Convolution of the theoretical cross-sections of D'Mello with our instrument function (i.e., the convolution of the heavy dashed and solid lines of Fig. 6). Circles connected by a light solid line: Relative integral cross-section (obtained by integrating D'Mello's data.)

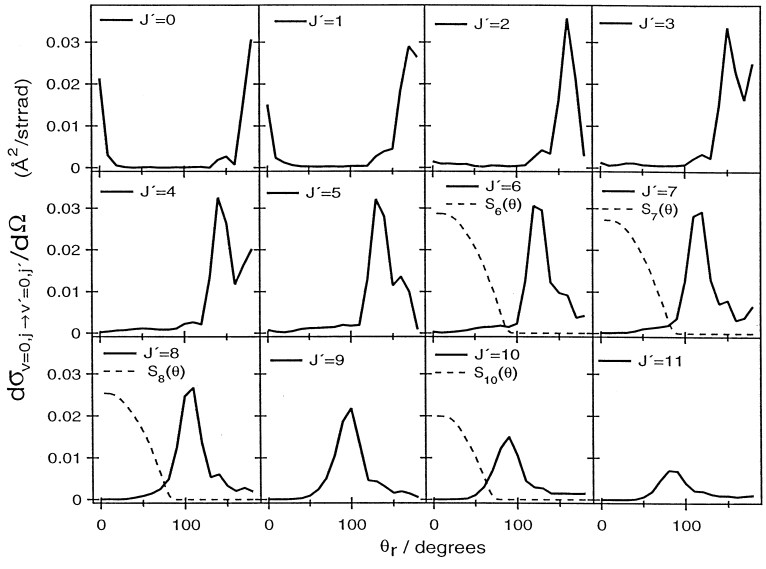

Fig. 6. Solid lines: State-to-state differential cross-sections of the $H + D_2(\nu = 0, j = 0) \rightarrow HD(\nu' = 0, j') + D$ reaction at 1.30 eV, as predicted by the quantum scattering calculations of Ref. [14]. Dashed lines: Relative sensitivity of our instrument to scattering angle.

data is good, but a chi-squared analysis yields $\chi^2 = 2.4$, indicating an unreasonably small (5%) probability that random errors alone account for the discrepancy between theory and experiment. One possible source of disagreement is inaccuracies in our Monte Carlo model. In particular, non-ideal ion optics or space-charge effects could cause slight differences in our sensitivity function. Examination of Fig. 6 shows that this possibility is particularly important for the $j' = 8$ and $j' = 10$ peaks where a small change in the maximum angle of sensitivity can lead to a large change in relative signal. We conclude that the scattering results of D'Mello and co-workers are consistent with our measurement.

6. Summary

The most significant contribution of the data presented in this work is that it demonstrates an ability to obtain sensitivity to angle-selected products of state-to-state reactions under conditions that yield high collision energy resolution. This ability is particularly important because the technique lends itself to the study of variety of state-to-state reactions as a continuous function of collision energy.

Our technique has been applied to the study of the $H + D_2 \rightarrow HD(v' = 0, j' = 6, 7, 8, 10)$ reaction at $E_{rel} = 1.275 \pm 0.011$ eV. At the present time our observations do not contradict the conclusion of Wrede and Schnieder [5] that the state-to-state differential cross-sections of the $H + D_2$ between 1.27 and 1.29 eV are well understood in terms of quantum-dynamical models that to do not take into account the geometric phase [5]. Specifically we have found that there is no dramatic difference between the forward-scattered cross-section of the $H + D_2 \rightarrow HD(v = 0, j' = 6, 7, 8, 10)$ predicted by theory at 1.30 eV and the actual probability for forward scattering at 1.275 eV.

Acknowledgements

This research is funded by the donors of the Petroleum Research Fund administered by the American Chemical Society (PRF-32187-G6), the National Research Council (NRC-6224), and the University of Oklahoma. The Monte Carlo simulations presented here were partially supported by an SUR grant from IBM to the University of Oklahoma. We are grateful to Mark Keil, Greg Parker, and Michael Morrison for useful discussions, and to Michael D'Mello for providing us with unpublished results.

Appendix A. Kinematic parameters for an ideal photoinitiated experiment

In an ideal photoinitiated measurement, the energetics of the reaction is completely predetermined. This requires that the translational temperature of the AX/BC gas mixture is cooled to absolute zero, the dissociation of AX leads to a monoenergetic A atom, the BC reactant and C atom product are in a single state, and only one energetic state of the AB product is probed. Under these conditions, laboratory-frame speed v_A of the A-atom photoproduct, the speed u of the center of mass, and the center-of-mass-frame speeds of the reactants and products (u_A, u_{BC}, u_{AB} and u_C) are all determined by conservation of energy and momentum [21]. Table 2 gives the value of these speeds and the collision energy in terms of mass factors, the dissociation energy D_0 of the AX precursor, the energy of the photolysis radiation $h\nu$, and the change in internal energy ΔE between the reactants and products.

Appendix B. Approximate analytical expressions for the distribution of collision energies in photoinitiated experiments

The distribution of initial velocities of the AX/BC gas mixture causes a spread in the relative energy that can be quite dramatic. In this section we derive simple analytical expressions for the distribution of collision energies in three variations of the photoinitiated studies bimolecular reactions: (1) photoinitiated experiments in a 'bulb' or flow characterized by a temperature T; (2) photoinitiated experiments in a collimated molecular beam for which the AB-product detection is insensitive to its velocity; and (3) photoinitiated experiments occurring in a collimated molecular beam for which only those AB products that travel radially outward from the beam are ob-

Table 2
Kinetic parameters for an ideal photoinitiated bimolecular reaction

Variable	Description	Eexpression for $AX + h\nu \rightarrow A + X\,(D_0)$, $A + BC \rightarrow AB + C\,(\Delta E)$	Value for $HI + h\nu(266\text{ nm}) \rightarrow H + I$, $H + D_2 \rightarrow HD(\nu' = 0, j' = 6) + D$
v_A	laboratory-frame photoproduct speed	$\left(\frac{2m_X(h\nu - D_0)}{m_A m_{AX}}\right)^{1/2}$	17.4 km s^{-1}
u	speed of the center of mass	$\left(\frac{2m_X m_A(h\nu - D_0)}{m_{ABC}^2 m_{AX}}\right)^{1/2}$	3.50 km s^{-1}
u_A	center-of-mass-frame speed of the A-atom reactant	$\left(\frac{2m_X m_{BC}^2(h\nu - D_0)}{m_{ABC}^2 m_A m_{AX}}\right)^{1/2}$	14.0 km s^{-1}
u_{BC}	center-of-mass-frame speed of the BC reactant	$\left(\frac{2m_X m_A(h\nu - D_0)}{m_{ABC}^2 m_{AX}}\right)^{1/2}$	3.50 km s^{-1}
E_{rel}	collision energy of the reaction	$\frac{m_X m_{BC}(h\nu - D_0)}{m_{AX} m_{ABC}}$	1.275 eV
u_{AB}	center-of-mass-frame speed of the AB product	$\left(\frac{2m_C(E_{rel} - \Delta E)}{m_{ABC} m_{AB}}\right)^{1/2}$	5.26 km s^{-1}
u_C	center-of-mass-frame speed of the C-atom product	$\left(\frac{2m_{AB}(E_{rel} - \Delta E)}{m_{ABC} m_C}\right)^{1/2}$	7.90 km s^{-1}
γ	u_{AB}/u	$\left(\frac{m_{BC} m_C(E_{rel} - \Delta E)}{m_{AB} m_A E_{rel}}\right)^{1/2}$	1.50
$v_{AB,max}$	laboratory-frame velocity of forward-scattered AB product	$u + u_{AB}$	8.77 km s^{-1}
$v_{AB,min}$	laboratory-frame velocity of backward-scattered AB product	$\lvert u - u_{AB}\rvert$	1.76 km s^{-1}

served. We note that the simplifications made in this section create a qualitatively correct, but unrealistically optimistic, prediction of the expected collision-energy resolution in a perpendicular beam experiment. The approximate expressions we obtain here provide a check of the detailed Monte Carlo analysis of Section 4 and provide convenient approximate expressions for use by theoreticians wishing to model experimental measurements. The convolution of energy-dependent theoretical cross-sections with the expressions given here will be valid provided (1) the photoproduct velocity is much greater than typical beam velocities, and (2) the theoretical predictions do not have structure on a scale much narrower than the energies corresponding to the translational temperature of the AX/BC gas mixture.

B.1. Case 1: The bulb experiment

This case was first derived by Chantry [34] and has been discussed extensively in Ref. [35]. It might at first appear that a small but finite translational temperature would limit the collision energy resolution to the temperature of the beam. The situation is actually far worse. In a realistic experiment, the collision energy E of a single collision is given by

$$E = \tfrac{1}{2}\mu|v_A - v_s|^2\,, \tag{B.1}$$

$$\tfrac{1}{2}\mu\left(v_A^2 + v_s^2 - 2v_A v_s\cos\xi\right), \tag{B.2}$$

$$\approx E_{rel} - \mu v_A v_s\cos\xi\,, \tag{B.3}$$

where $\mu = m_A m_{BC}/(m_A + m_{BC})$ is the reduced mass of the bimolecular system, v_A is the typically fast

AX-molecular-frame speed of the photoproduct, $\boldsymbol{v}_s = \boldsymbol{v}_{BC} - \boldsymbol{v}_{AX}$ is the difference between the velocity of the diatomic reactant and the velocity of the photolytic precursor, and ξ is the angle between $\boldsymbol{v}_A$ and $\boldsymbol{v}_s$. Whereas in an ideal experiment the value of $\boldsymbol{v}_s$ is zero, in general $\boldsymbol{v}_s$ has a thermal distribution of values. The term in Eq. (B.2) that is proportional to v_s^2 will therefore lead to a small spread in the collision energy that is determined by the temperature of the gas mixture. The cross term in Eq. (B.2) is not, however, small. This term is proportional to the fast speed v_A and therefore leads to a 'superthermal' spread in the collision energy [35]. The distribution of $u_s = v_s \cos\xi$ is the distribution of AX–BC velocities parallel to the direction of $\boldsymbol{v}_A$. For the case of a conventional photoinitiated experiment in a flow or bulb, the distribution of u_s is given by a Maxwell–Boltzmann distribution of temperature T:

$$P(u_s) = \frac{1}{\sqrt{\pi}\,\Delta v_s}\exp\left(-u_s^2/\Delta v_s^2\right), \tag{B.4}$$

where

$$\Delta v_s = \sqrt{\frac{2k_BT}{\mu'}}\ . \tag{B.5}$$

Here $\mu' = m_{AX}m_{BC}/(m_{AX}+m_{BC})$ is the reduced mass of the precursor and BC reactant. If we assume the approximation of Eq. (B.3), $E_{rel} - E \approx \mu v_A u_s$, and the expected distribution of collision energies can be found by a simple change of variables in Eq. (B.4):

$$P_{bulb}(E) \approx \frac{1}{\sqrt{\pi}\,\Delta E_{bulb}}\exp\left[-(E-E_{rel})^2/\Delta E_{bulb}^2\right], \tag{B.6}$$

where

$$\Delta E_{bulb} = \mu v_A \Delta v_s\,. \tag{B.7}$$

Eqs. (B.6) and (B.7) are equivalent to the result of eq. 5 of Ref. [35].

The width ΔE_{bulb} of this Gaussian distribution can be found by finding Δv_s from Eq. (B.5) and v_A from Table 2. For illustrative purposes, we pick a value T that corresponds to the 330 m s^{-1} FWHM spread in the beam velocity in our study of the H + D_2 reaction. To this end, we multiply this factor of 330 m s^{-1} $\sqrt{2}$ by to obtain the spread in relative speeds between the D_2 and HI molecules and divide by $2\sqrt{\ln 2}$ to convert from FWHM to the scaling used in Eq. (B.6). This simple manipulation leads to a value of $\Delta v_s = 280$ m s^{-1} and a temperature of 18.6 K. Using this temperature and the value $v_A =$ 17.5 km s^{-1} from Table 2, we find $\Delta E_{bulb} = \mu\Delta v_s v_A = 41$ meV. A Gaussian parameterized by this value of ΔE_{bulb} is compared to our Monte Carlo simulation in Fig. 5.

B.2. Case 2: Photoinitiated experiments in a collimated molecular beam for which the AB product detection is insensitive to the velocity of the product

In many photoinitiated experiments, the AX/BC gas mixture may be expanded from a high- into a low-pressure vacuum system where the photoinitiated reaction takes place. If the pressure in the vacuum system is low enough that the mean free path is long compared to the physical dimensions of the system (typically $P < 10^{-4}$ Torr), the gas molecules at any point within the path of the expansion will have velocities directed directly away from the source, i.e., the gas molecules in any given region of space travel in a well-defined direction. Thus, instead of blurring the collision energy by a three-dimensional Maxwell–Boltzmann distribution of initial velocities, as in Section B.1, we must consider the effect of a Maxwell–Boltzmann distribution of velocities along only one axis.

To determine the distribution of collision energies we note that Eq. (B.3) still applies. Now the angle ξ is the angle between the velocity $\boldsymbol{v}_A$ of the photoproduct and the direction of the molecular beam. If, for simplicity, we assume an isotropic dissociation of A-atom velocities, then the distribution of $\cos\xi$ will be uniform from -1 to 1. Convoluting this uniform distribution with the distribution in v_s in Eq. (B.3) allows us to find the expected spread in collision energies, $P_{1D}(E)$:

$$\begin{aligned} P_{1D}(E) &= \frac{1}{2\pi^{1/2}}\int_{-\infty}^{\infty}\int_{-1}^{-1}\exp\left(-v_s^2/\Delta v_s^2\right)\delta \\ &\quad\times(E - E_{rel} - \mu v_A v_s\cos\xi)\,\mathrm{d}\cos\xi\,\mathrm{d}v_s \\ &= \frac{1}{\Delta E_{bulb}} f_{1D}\left(\frac{E-E_{rel}}{\Delta E_{bulb}}\right), \end{aligned} \tag{B.8}$$

where

$$f_{1D}(x) = \frac{-1}{2\pi^{1/2}}\mathrm{Ei}(-x^2)\,. \qquad (B.9)$$

Here Ei is the exponential integral function. The distribution $P_{1D}(E)$ is plotted in Fig. 5 for $E_{rel} = 1.275$ eV and $\Delta E_{bulb} = 41$ meV. We note that $P_{1D}(E)$ is more sharply peaked than the Gaussian distribution in a photoinitiated experiment carried out in a bulb. This increase in resolution has been gained by defining a unique direction of flow.

B.3. Case 3: Photoinitiated experiments in a molecular beam with v_A constrained to be radial

We now derive the distribution of collision energies for an experiment in which only products that travel perpendicular to a laser beam are detected. Fig. 1 helps to determine the parameters that must be considered to achieve this goal. Although measurement of the speed v_{AB} of a state-selected product determines the center-of-mass-frame scattering angle θ_r, it does not determine the azimuthal angle ϕ between the scattering plane and the direction of $\boldsymbol{v}_{AB}$. Nor do we determine the relative velocity v_s between the AX precursor and BC reactant. If these two parameters were known, then the collision energy could be determined:

$$E \approx E_{rel} - \mu v_A v_s \cos\xi\,, \qquad (B.10)$$

$$= E_{rel} - \mu v_A v_s \cos\beta \sin\phi\,. \qquad (B.11)$$

Here the cosine of the angle β can be expressed in terms of the scattering angle and the speeds u_{AB} and u by application of the law of cosines:

$$\cos\beta = \frac{\sin\theta_r}{\sqrt{1+\gamma^{-2}+2\gamma^{-1}\cos\theta_r}}\,, \qquad (B.12)$$

where $\gamma = u_{AB}/u$ is defined in Table 2. Eq. (B.11) can be used to determine the distribution of the collision energies from the distribution of values of ϕ and v_s. To keep matters simple, we assume an isotropic photodissociation. For this case, ϕ of Eq. (B.11) takes on a uniform distribution of values from 0 to 2π. The distribution of relative velocities v_s in the beam is assumed to be the Gaussian form of Eq. (B.3). The result of convoluting these distributions in ϕ and v_s with the expression of Eq. (B.10) is the following angle-dependent collision energy resolution:

$$P_\perp(E) = \frac{1}{2\pi^{3/2}}\int_{-\infty}^{\infty}\int_0^{\pi}\exp\left(-v_s^2/\Delta v_s^2\right)\delta \times\left(E - E_{rel} - \mu v_A v_s\cos\beta\sin\phi\right)\mathrm{d}\phi\,\mathrm{d}v_s\,,$$

$$= \frac{1}{\Delta E} f_\perp\left(\frac{E-E_{rel}}{\Delta E}\right), \qquad (B.13)$$

where

$$f_\perp(x) = \frac{1}{\pi^{3/2}}\exp\left(-x^2/2\right)K_0\left(x^2/2\right) \qquad (B.14)$$

and

$$\Delta E = \frac{\mu v_A \Delta v_s \sin\theta_r}{\sqrt{1+\gamma^{-2}+2\gamma^{-1}\cos\theta_r}}\,. \qquad (B.15)$$

Here $K_0(x)$ is the modified Bessel function.

The nature of the distribution function for $P_\perp(E)$ is strikingly different from $P_{bulb}(E)$. The perpendicular beam distribution is sharply peaked and not at all Gaussian, as shown in Fig. 8. In addition, the distribution of collision energies is highly dependent on the scattering angle of the reaction. For forward- and backward-scattered products, the distribution

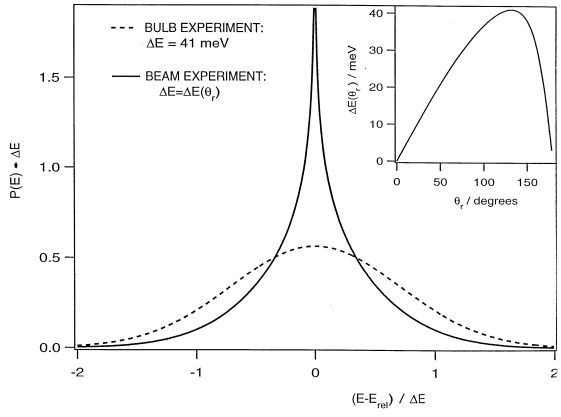

Fig. 8. Approximate distribution of $H–D_2$ collision energies occurring in the $HI + h\nu(266\,nm) \rightarrow H + I(^2P_{3/2})$, $H + D_2 \rightarrow HD + D$ reaction sequence. Dotted line: collision energy resolution for the case that the reaction sequence occurs in a 18.6 K HI/D_2 gas mixture. Solid line: Scattering-angle-dependent resolution for the case that the HD product traveling radially from a molecular beam with $\Delta v_s = 280$ m s^{-1} is observed (see text). Inset: Dependence of the resolution ΔE on scattering angle.

function $P_{\perp}(E)$ becomes a Dirac delta function. To see why this occurs, one need only examine Fig. 1. For the case of forward- and backward-scattered products, the relative velocity becomes exactly perpendicular to the beam. Thus the cross term of Eq. (B.2) vanishes, resulting in extremely precise determination of the collision energy.

References

[1] A. Kuppermann, Y.-S.M. Wu, Chem. Phys. Lett. 241 (1995) 229.
[2] R. Fei, X.S. Zheng, G.E. Hall, J. Phys. Chem. A 101 (1997) 2541.
[3] Y.-T. Hsu, J.-H. Wang, K. Liu, J. Chem. Phys. 107 (1997) 2351.
[4] L. Schnieder, K. Seekamp-Rahn, J. Borkowski, E. Wrede, K.H. Welge, F.J. Aoiz, L. Banares, M.J. D'Mello, V.J. Herrero, V.S. Rabanos, R.E. Wyatt, Science 269 (1995) 207.
[5] E. Wrede, L. Schnieder, J. Chem. Phys. 107 (1997) 786.
[6] E. Wrede, L. Schnieder, K.H. Welge, F.J. Aoiz, L. Banares, V.J. Herrero, B. Martinez-Haya, V.S. Rabanos, J. Chem. Phys. 106 (1997) 7862.
[7] L. Schnieder, K. Seekamp-Rahn, E. Wrede, K.H. Welge, J. Chem. Phys. 107 (1997) 6175.
[8] D.E. Adelman, N.E. Shafer, D.A.V. Kliner, R.N. Zare, J. Chem. Phys. 97 (1992) 7323.
[9] D. Neuhauser, R.S. Judson, D.J. Kouri, D.E. Adelman, N.E. Shafer, D.A.V. Kliner, R.N. Zare, Science 257 (1992) 519.
[10] Y.i.S.M. Wu, A. Kuppermann, Chem. Phys. Lett. 201 (1993) 178.
[11] M.J. D'Mello, D.E. Manolopoulos, R.E. Wyatt, J. Chem. Phys. 94 (1991) 5985.
[12] F.J. Aoiz, L. Banares, M.J. D'Mello, V. Herrero, V.S. Rabanos, L. Schnieder, R.E. Wyatt, J. Chem. Phys. 101 (1994) 5781.
[13] M.J. D'Mello, D.E. Manopoulos, R.E. Wyatt, Science 102 (1994) .
[14] M.J. D'Mello, personal communication on ''Differential cross sections obtained using the scattering code'', by M.J. D'Mello, D.E. Manolopoulos, R.E. Wyatt, J. Chem. Phys. 94 (1991) 5985.
[15] R.D. Levine, R.B. Bernstien, Molecular Reaction Dynamics and Chemical Reactivity, Oxford University Press, New York, 1987.
[16] G.E. Hall, presented at 12th Combustion Res. Conf., Tahoe City, CA, 1990.
[17] N.E. Shafer, Ph.D. Thesis, Columbia University, New York, 1990.
[18] M. Brouard, S.P. Duxon, P.A. Enriquez, R. Sayos, J.P. Simons, J. Phys. Chem. 95 (1991) 8169.
[19] M. Brouard, S.P. Duxon, P.A. Enriquez, J.P. Simons, J. Chem. Phys. 97 (1992) 7414.
[20] M. Brouard, S.P. Duxon, P.A. Enriquez, J.P. Simons, J. Chem. Soc., Faraday Trans. 89 (1993) 1435.
[21] N.E. Shafer, A.J. Orr-Ewing, W.R. Simpson, H. Xu, R.N. Zare, Chem. Phys. Lett. 212 (1993) 155.
[22] W.R. Simpson, A.J. Orr-Ewing, R.N. Zare, Chem. Phys. Lett. 212 (1993) 163.
[23] M. Brouard, S.P. Duxon, J.P. Simons, Isr. J. Chem. 98 (1994) 67.
[24] H.L. Kim, M.A. Wickramaaratchi, X. Zheng, G.E. Hall, J. Chem. Phys. 101 (1994) 2033.
[25] N.E. Shafer, H. Xu, R.P. Tuckett, M. Springer, R.N. Zare, J. Phys. Chem. 98 (1994) 3369.
[26] N.E. Shafer-Ray, A.J. Orr-Ewing, R.N. Zare, J. Phys. Chem. 95 (1995) 7591.
[27] H. Xu, N.E. Shafer-Ray, F. Merkt, D.J. Hughes, M. Springer, R.P. Tuckett, R.N. Zare, J. Chem. Phys. 103 (1995) 5158.
[28] A.J. Alexander, F.J. Aoiz, L. Banares, M. Brouard, V.J. Herrero, J.P. Simons, Chem. Phys. Lett. 278 (1997) 313.
[29] W. Simpson, P. Rakitzis, A. Kandel, J. Chem. Phys. 106 (1997) 5961.
[30] W. Demtroder, Laser Spectroscopy, 5, Springer, New York, 1982.
[31] S.L. Anderson, G.D. Kubiak, R.N. Zare, Chem. Phys. Lett. 105 (1984) 22.
[32] K. Dharmasena, J. Jefferies, G. Mu, J. Young, B. Bergeron, R. Littell, N. Shafer-Ray, Rev. Sci. Instrum. 69 (1998) 2880.
[33] L.J. Danielson, M. Keil, J. Chem. Phys. 88 (1988) 851.
[34] P.J. Chantry, J. Chem. Phys. 55 (1971) 2746.
[35] W.J. van der Zande, R. Zhang, R.N. Zare, K.G. McKendrick, J.J. Valentini, J. Phys. Chem. 96 (1991) 8205.